Decoherence of high-energy electrons in weakly disordered quantum Hall edge states

Simon E. Nigg[1*] and Anders Mathias Lunde[2]
[1]*Department of Physics, University of Basel, Klingelbergstrasse 82, 4056 Basel, Switzerland and*
[2]*Center for Quantum Devices, Niels Bohr Institute, University of Copenhagen, Universitetsparken 5, 2100 Copenhagen, Denmark*
(Dated: June 29, 2016)

We investigate theoretically the phase coherence of electron transport in edge states of the integer quantum Hall effect at filling factor $\nu = 2$, in the presence of disorder and inter-edge state Coulomb interaction. Within a Fokker-Planck approach, we calculate analytically the visibility of the Aharonov-Bohm oscillations of the current through an electronic Mach-Zehnder interferometer. In agreement with recent experiments, we find that the visibility is independent of the energy of the current-carrying electrons injected high above the Fermi sea. Instead, it is the amount of disorder at the edge that sets the phase space available for inter-edge state energy exchange and thereby controls the visibility suppression.

PACS numbers: 73.23.-b, 73.43.Cd, 72.70.+m

arXiv:1606.08574v1 [cond-mat.mes-hall] 28 Jun 2016

Phase coherent electron transport at the edge of a two dimensional electron gas (2DEG) is a fascinating topic in condensed matter physics, both because of its fundamental role in unveiling new correlated states of matter [1, 2], as well as for its practical implications for electronic quantum information processing [3–6], and the emerging field of quantum coherent thermo-electrics [7, 8]. Although among the oldest quasi-one dimensional systems to have been discovered [9–13], edge states (ESs) in the integer quantum Hall regime are still not fully understood theoretically. In particular, despite intense activity [14–35], our understanding of the dominant decoherence mechanism in transport through ESs is incomplete. This is illustrated by the recent experiment of Tewari et al. [33], in which it was observed that decoherence of high energy electrons sent through a Mach Zehnder interferometer (MZI), formed with two co-propagating ESs at filling factor $\nu = 2$, does not depend on the energy of the injected electrons. This contradicts theoretical predictions based on the Luttinger-liquid model for one dimensional, translationally invariant systems [25–27, 33, 34]. Disorder, however, is conspicuous for its absence in these approaches. While macroscopic phenomena, such as the quantization of the Hall resistance, are robust to disorder, more subtle quantum effects, such as coherent energy exchange and phase coherence between co-propagating ESs, can be expected to be sensitive to even weak disorder at the edge of a high mobility 2DEG [36].

In this work, we show that by taking into account disorder, which breaks translation invariance along the edge, a gapless continuum of low energy quasi-particle excitations emerges. Their dynamics provides a simple physical picture of interaction-induced decoherence, which in turn provides a natural explanation for the experimental findings of [33]. Our theory has previously also been successfully applied to energy relaxation in out-of-equilibrium ESs [23, 37]. In particular, in [37], we showed that energy relaxation of electrons injected high above the Fermi sea into the outermost of two co-propagating, interacting and *weakly disordered* ESs, can be described in terms of a drift-diffusion process of their energy distribution function: As the injected electrons propagate along the outer ES, they loose energy and their energy distribution moves towards the Fermi sea with a *constant* energy drift velocity and broadens at a position-dependent rate. The latter is determined by the induced heating of the inner ES, which absorbs the energy lost by the injected electrons and subsequently redistributes part of this energy to the Fermi sea of the outer ES. The central new idea of the present work is that, given a relation between the energy and the phase of a propagating electron, knowing the dynamics of the energy distribution function enables us to calculate the statistics of the interaction-induced phase fluctuations. In the absence of extrinsic dephasing mechanisms, the latter fully determines the coherence of electron transport.

Explicitly, we find that the interaction-induced suppression of the visibility of the current interference fringes through an electronic MZI (see Fig. 1 (a)), is determined by the temperature of the electronic system, the drift velocity of the energy distribution of the electrons injected into the outer ES and the heating of the Fermi sea of the inner ES. Importantly, none of these quantities depend on the injection energy of the electrons, resulting in dephasing that is independent of the injection energy, inline with the experiment of Tewari et al. [33]. Rather, the amount of dephasing is governed by the amount of disorder, which sets the available phase space for inelastic, non-momentum conserving, electron-electron scattering. This result suggests that disorder along the edges of a patterned 2DEG plays a more important role, with regards to energy relaxation and decoherence of ESs, than hitherto assumed.

The system we consider is that of [33] and is depicted schematically in Fig. 1. It consists of two co-propagating chiral ESs, one of which is split via two quantum point contacts (QPCs) such as to form a MZI. Furthermore, a quantum dot (QD) side-coupled to the sample edge at the input of the interferometer is used for energy-resolved injection of electrons into the outer ES with an average energy E_0 much larger than the Fermi energy μ_o of the outer ES as compared with the initial energy spread Γ_0 of the injected electrons, i.e. $E_0 - \mu_o \gg \Gamma_0$ (see Fig. 1 (b)). If all contacts, with the exception of the source, are kept at the same voltage, the DC current $I(\Phi, \Delta L)$ measured at the output port of the interferometer will stem exclusively from electrons injected into the

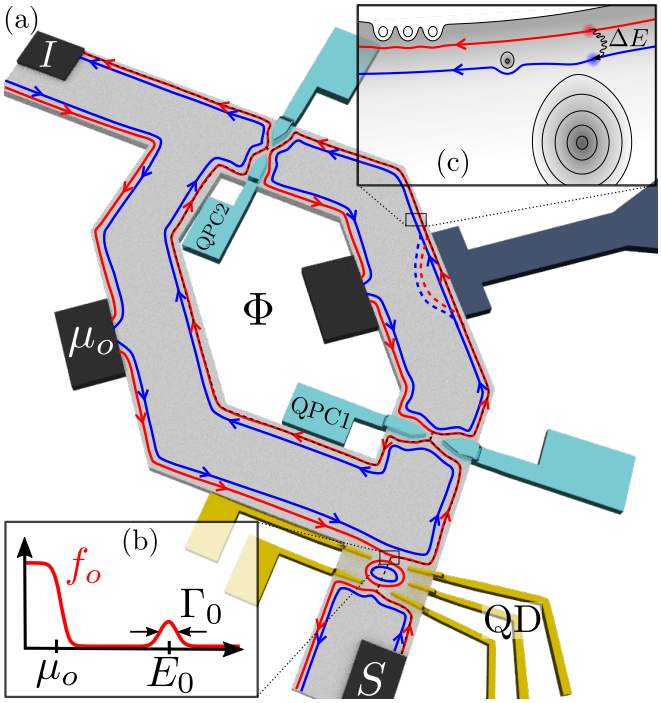

FIG. 1. Schematics of a Mach-Zehnder interferomter realized in [33] with ESs of the integer quantum Hall effect at filling factor $\nu = 2$. (a) The outer (inner) chiral ES is shown by a solid red (blue) line following the edge of the patterned 2DEG structure (light gray area). The arrows indicate the propagation direction which is determined by the orientation of the magnetic field perpendicular to the 2DEG (not shown). A quantum dot (bottom right) is used for energy-resolved injection of high-energy electrons, with mean energy E_0, into the outer ES by filtering the electrons emitted at the source marked with S. This creates a non-equilibrium energy distribution in the outer ES composed of a Fermi sea part and a narrow bump around E_0 as shown in (b). An injected electron is scattered at two QPCs and can follow two possible paths, marked by dashed (black) lines, before exiting the interferometer at the top left corner where the current is measured. Interference between the current amplitudes corresponding to these two paths can be modulated either by threading a magnetic flux Φ through the loop created by the two paths or, as in the experiment [33], by applying a local gate voltage along one arm, in order to modify the path length difference ΔL (dark blue side gate). The visibility of the current oscillations in either ΔL or Φ, is suppressed by inelastic scattering between electrons in the inner and outer ESs, which follow the equipotential lines of the disordered confinement potential [36] (c). In the case of unequal arm lengths, additional dephasing takes place due to the initial energy spread Γ_0 of the injected electrons (b).

outer ES via the QD energy filter. The flux dependence of this current, is thus a sensitive probe of phase coherence along the outer ES. Instead of varying a magnetic flux Φ through the loop formed by the two arms of the interferometer, one may alternatively, as in the experiment [33], vary the path length difference $\Delta L = L_1 - L_2$, e.g. by applying a gate voltage to one of the arms. A similar setup, albeit with a simpler topology, has been used previously to investigate energy relaxation in out-of-equilibrium ESs [20, 21].

We focus on Coulomb mediated energy exchange between the inner and outer co-propagating ESs, without particle exchange. This is reasonable in the absence of magnetic impurities, since the two edge states have opposite spins and therefore particle exchange would require a spin flip. In analogy with the non-interacting scattering theory [38, 39], the contribution from the outer ES to the current at the output port of the MZI can then be written as

$$I(\Phi, \Delta L) = \frac{e}{h} \int dE b_0(E) \langle |r_1 r_2 + t_1 t_2 e^{i\phi_E}|^2 \rangle . \qquad (1)$$

Here $b_0(E)$ denotes the energy distribution function of the electrons injected via the QD and centered at E_0. r_i (t_i) is the real reflection (transmission) probability amplitude at the i-th QPC, and ϕ_E denotes the relative phase acquired by an electron injected with energy E but traversing different arms of the MZI. Crucially, the phase ϕ_E is a random variable that depends on the injection energy E, and on the random energy exchange events between injection and detection. The brackets $\langle \cdot \rangle$ denote averaging over all possible realizations of scattering events. Assuming that the energy dependence of the transmission and reflection amplitudes through the QPCs around the injection energy is negligible [18, 33], it follows from Eq. (1) that the coherent part of the current is given by

$$I_\varphi = \frac{e}{h}(r_1 r_2 t_1 t_2) \int dE b_0(E) \langle e^{i\phi_E} + e^{-i\phi_E} \rangle . \qquad (2)$$

Hence, assuming $b_0(E)$ is known, our task is reduced to computing the average of $\exp(i\phi_E)$ over scattering events.

For the case of a linear dispersion considered here, the phase acquired by an electron propagating in the outer ES along one of the arms of the interferometer (say $l = 1$ for the upper and $l = 2$ for the lower arm according to Fig. 1) is simply given by

$$\phi_E^{(l)}(x) = \frac{1}{\hbar v_o} \int_0^x dy E(y), \qquad (3)$$

where v_o is the velocity of the electron in the outer ES and $E(y)$ denotes the energy of the electron at position y in arm l, given the initial energy $E(0) = E$. The relative phase at the detector is then simply given by

$$\phi_E = \phi_E^{(1)}(L_1) - \phi_E^{(2)}(L_2) + 2\pi\Phi/\Phi_0, \qquad (4)$$

where L_l is the length of interferometer arm l, possibly including a gate induced path length variation. Because electrons on different arms do not interact, owing to screening and a sufficiently large spatial separation, the average over scattering events factorizes

$$\langle e^{i\phi_E} \rangle = \langle \exp(i\phi_E^{(1)}(L_1)) \rangle \langle \exp(-i\phi_E^{(2)}(L_2)) \rangle e^{2\pi i \Phi/\Phi_0}, \qquad (5)$$

and it is sufficient to evaluate the interaction-induced coherence suppression factor $\mathcal{F}_E^{(l)}(x) \equiv \langle \exp(i\phi_E^{(l)}(x)) \rangle$ for one arm. From now on, we thus suppress the arm label l.

Our starting point for evaluating $\mathcal{F}_E(x)$, is the kinetic Boltzmann equation for the energy distribution functions f_α of the inner ($\alpha = i$) and outer ($\alpha = o$) ESs

$$v_\alpha \partial_x f_\alpha(E,x) = \mathcal{I}_{Ex\alpha}\left[f_\alpha, f_{\bar{\alpha}}\right]. \tag{6}$$

The term on the right-hand side is the difference of in-scattering ($\{E'\} \to E$) and out-scattering ($E \to \{E'\}$) energy exchange processes between the inner and outer ESs [40]. Here and below, we use the shorthand notation $\overline{\alpha} = \delta_{\alpha i} o + \delta_{\alpha o} i$. If both energy and momentum are conserved, then two-body collisions cannot change the distribution function in one dimension, as long as $v_i \neq v_o$, [41]. However, disorder along the edge breaks translation invariance such that inelastic electron-electron scattering without momentum conservation becomes possible. Thereby, an effective interaction is induced and the phase-space for energy exchange between electrons in the inner and outer ESs opens up. In contrast to collective excitations in a finite length system [42], these excitations are gapless. As shown in [23, 37, 43], this situation is described by Eq. (6) with the collision integral

$$\begin{aligned}\mathcal{I}_{Ex\alpha}[f_\alpha, f_{\bar{\alpha}}] = v_\alpha \gamma \int d\omega e^{-(\omega/\Delta E)^2} \\ \times \Big\{ f_\alpha(E+\omega,x)\left[1-f_\alpha(E,x)\right] D_{\bar{\alpha}}(\omega,x) \\ - f_\alpha(E,x)\left[1-f_\alpha(E+\omega,x)\right] D_{\bar{\alpha}}(-\omega,x)\Big\},\end{aligned} \tag{7}$$

where γ is the effective inter-ES interaction strength, ΔE is the energy scale for the amount of energy exchanged per non-momentum conserving collision [43], and

$$D_\alpha(\omega,x) = \int dE f_\alpha(E-\omega,x)(1-f_\alpha(E,x)). \tag{8}$$

The inner ES is initially in thermal equilibrium so that $f_i(E,0) = 1/[1+\exp((E-\mu_i)/k_{\text{B}}T)]$. Furthermore, because we consider electrons injected high above the Fermi sea in the outer ES ($E_0 - \mu_o \gg \Gamma_0$), we can split the distribution function in the outer ES into two essentially non-overlapping contributions

$$f_o(E,x) = \mathfrak{f}_o(E,x) + b(E,x), \tag{9}$$

where $\mathfrak{f}_o(E, x=0) = 1/[1+\exp(\beta(E-\mu_o))]$ and $b(E,x)$ is the energy distribution of the injected electrons at position x with boundary condition $b(E,0) = b_0(E)$. If, as in the experiment [33], the transmission probability through the QD is small, then $b(E,x) \ll 1$. Consequently, we can neglect, in the collision integral, all terms of order $O(b^2, b\mathfrak{f}_o)$. Finally, since we are interested in the limit of weak disorder, ΔE is taken to be the smallest energy scale, e.g. $\Delta E \ll k_{\text{B}}T, \Gamma_0$. These steps allow us to derive, from the kinetic equation, the following set of coupled Fokker-Planck equations [37]

$$\partial_x b(E,x) = \eta\left\{\partial_E b(E,x) + D_i(0,x)\partial_E^2 b(E,x)\right\}, \tag{10a}$$

$$\begin{aligned}\partial_x f_i(E,x) = \eta \frac{N_b}{\rho_o}\partial_E^2 f_i(E,x) \\ + \eta\left\{\left[1-2f_i(E,x)\right]\partial_E f_i(E,x) + \mathfrak{D}_o(0,x)\partial_E^2 f_i(E,x)\right\},\end{aligned} \tag{10b}$$

$$\partial_x \mathfrak{f}_o(E,x) = \eta\left\{\left[1-2\mathfrak{f}_o(E,x)\right]\partial_E \mathfrak{f}_o(E,x) + D_i(0,x)\partial_E^2 \mathfrak{f}_o(E,x)\right\}. \tag{10c}$$

Here $\eta = (\sqrt{\pi}/4)\gamma(\Delta E)^3$ is the energy drift velocity, ρ_o is the density of states in the outer ES, $N_b = \rho_o \int dE b_0(E)$, is the mean number of injected electrons and $\mathfrak{D}_o(\omega,x) = \int dE \mathfrak{f}_o(E-\omega,x)\left[1-\mathfrak{f}_o(E,x)\right]$.

The Fokker-Planck equation (10a) is equivalent [44] to the Itô stochastic differential equation

$$dE = -\eta dx + g(x)\mathrm{d}W_x, \tag{11}$$

where $g(x) = \sqrt{2\eta D_i(0,x)}$ and $\mathrm{d}W_x$ is a Wiener process. The random energy of an electron injected at $x = 0$ with energy E, is obtained by integrating Eq. (11) and using the initial condition $E(x=0) = E$:

$$E(x) = E - \eta x + \int_0^x g(y)\mathrm{d}W_y. \tag{12}$$

The last term in Eq. (12) is a stochastic Itô integral. By applying the Itô calculus ($\langle \mathrm{d}W_x \mathrm{d}W_{x'}\rangle = \delta(x-x')dx$, $\langle \mathrm{d}W_x\rangle = 0$), we find the mean and variance ($\mathrm{Var}[\cdot] = \langle(\cdot)^2\rangle - \langle\cdot\rangle^2$) of the energy at position x as

$$\langle E(x)\rangle = E - \eta x, \tag{13a}$$

$$\mathrm{Var}[E(x)] = 2\eta \int_0^x D_i(0,y)dy. \tag{13b}$$

Note that averaging Eq. (13a) over the injection energy using the probability density $(\rho_o/N_b)b_0(E)$ yields $\langle\langle E(x)\rangle\rangle_0 = E_0 - \eta x$, which explains why η is called the energy drift velocity of the energy distribution of the injected electrons. Because of Eq. (13b), we further call $2\eta D_i(0,x)$ the dynamic diffusion coefficient [37]. According to Eq. (3), the phase of the electron at position x is now given by

$$\phi_E(x) = \frac{1}{\hbar v_o}\left(Ex - \frac{1}{2}\eta x^2\right) + \frac{1}{\hbar v_o}\int_0^x \int_0^y g(z)\mathrm{d}W_z dy. \tag{14}$$

Using again the Itô calculus [43], the last integral can be rewritten as

$$\int_0^x \int_0^y g(z)\mathrm{d}W_z dy = \int_0^x (x-y)g(y)\mathrm{d}W_y, \tag{15}$$

from which it follows that the variance of the phase is

$$\delta\phi^2(x) \equiv \mathrm{Var}\left[\phi_E(x)\right] = \frac{2\eta}{(\hbar v_o)^2}\int_0^x (x-y)^2 D_i(0,y)dy. \tag{16}$$

Because the fluctuating part of the phase is itself a Gaussian random variable with zero mean, we can use the identity $\langle \exp(i\phi)\rangle = \exp(i\langle\phi\rangle)\exp(-\delta\phi^2/2)$, and the interaction-induced dephasing factor is given by

$$\mathcal{F}_E(x) = \exp\left(\frac{i}{\hbar v_o}\left[Ex - \frac{1}{2}\eta x^2\right]\right)\exp\left(-\frac{\delta\phi^2(x)}{2}\right). \quad (17)$$

Eq. (17) together with Eq. (16) are the main analytic results of this work. They link the interaction-induced phase coherence suppression factor of the outer ES to the relaxation induced smearing of the energy distribution of the inner ES, quantified by $D_i(0,x)$ (see Eq. (8)). Importantly, the latter is independent of the injection energy as shown below. Combining Eqs. (2), (4), (5) and (17), we obtain an explicit expression for the coherent current through the interferometer

$$I_\varphi(\Phi,\Delta L) = \frac{2e}{h}\frac{N_b}{\rho_o}(r_1 r_2 t_1 t_2)B_0(\Delta L)e^{-\frac{1}{2}\left[\delta\phi^2(L_1)+\delta\phi^2(L_2)\right]} \quad (18)$$
$$\times\cos\left(\frac{E_0\Delta L}{\hbar v_o} - \frac{\eta\left(L_1^2 - L_2^2\right)}{2\hbar v_o} + \frac{2\pi\Phi}{\Phi_0}\right).$$

Here the factor $B_0(\Delta L) = \frac{\rho_o}{N_b}\int dE b_0(E+E_0)e^{i\frac{E\Delta L}{\hbar v_o}}$ characterizes the dephasing due to the initial energy spread of the injected electrons for finite path length difference, and the exponential factor quantifies the interaction-induced dephasing. For an initial Gaussian energy distribution of the form $b_0(E) = \frac{N_b}{\rho_o\sqrt{\pi}\Gamma_0}\exp\left[(E-E_0)^2/\Gamma_0^2\right]$, we have $B_0(\Delta L) = \exp\left[-\left(\frac{\Gamma_0\Delta L}{2\hbar v_o}\right)^2\right]$. For an initial distribution of the form $b_0(E) = \frac{N_b}{4\Gamma_0\rho_o}\cosh^{-2}\left(\frac{E-E_0}{2\Gamma_0}\right)$, which, with $\Gamma_0 = k_B T$, is appropriate for injection through a thermally broadened QD level [33], we have $B_0(\Delta L) = \frac{\pi\Gamma_0\Delta L}{2\hbar v_o}\mathrm{csch}\left(\frac{\pi\Gamma_0\Delta L}{\hbar v_o}\right)$. In both cases $B_0(\Delta L\to 0)\to 1$ as expected. The experimentally relevant visibility of the current interference $\mathcal{V} \equiv (I_{\mathrm{MAX}} - I_{\mathrm{MIN}})/(I_{\mathrm{MAX}} + I_{\mathrm{MIN}})$ is found by extremizing the cosine in Eq. (18) over either Φ or variations of the path length difference ΔL [45] and reads

$$\mathcal{V} = \frac{2r_1 r_2 t_1 t_2}{(r_1 r_2)^2 + (t_1 t_2)^2}B_0(\Delta L)e^{-\frac{1}{2}\left[\delta\phi^2(L_1)+\delta\phi^2(L_2)\right]}. \quad (19)$$

To obtain the variance of the phase fluctuations, we need to evaluate the function $D_i(0,x)$, i.e. solve Eqs. (10b) and (10c). A thorough discussion of these equations can be found in [37], where it was shown that an approximate solution, takes the form of an effective temperature ansatz for $f_i(E,x)$ and $\mathfrak{f}_o(E,x)$:

$$f_i^F(E,x) = \frac{1}{1+\exp\left[\frac{E-\mu_i}{k_B T_i(x)}\right]}, \quad (20a)$$

$$\mathfrak{f}_o^F(E,x) = \frac{1}{1+\exp\left[\frac{E-\mu_o}{k_B T_o(x)}\right]}. \quad (20b)$$

From Eq. (8) it immediately follows that, within the effective temperature approximation, $D_i(0,x) = k_B T_i(x)$. The coupled Fokker-Planck Eqs. (10b) and (10c) now reduce to coupled ordinary differential equations for $T_i(x)$ and $T_o(x)$:

$$k_B\partial_x T_i(x) = \eta\frac{3}{\pi^2}\left(\frac{N_b/\rho_o}{k_B T_i(x)} + \frac{T_o(x)}{T_i(x)} - 1\right), \quad (21a)$$

$$k_B\partial_x T_o(x) = \eta\frac{3}{\pi^2}\left(\frac{T_i(x)}{T_o(x)} - 1\right). \quad (21b)$$

In the case of interest here, the Fermi seas of the inner and outer ESs initially have the same temperature $T_i(0) = T_o(0) = T$. Moreover, since we are working in the limit of weak disorder where $\Delta E \ll k_B T$, it is reasonable to expect that the difference between the two effective temperatures $T_d(x) = (T_i(x) - T_o(x))/2$ remains small compared with the sum of the temperatures $T_s(x) = (T_i(x) + T_o(x))/2$ at all positions. From this assumption, one can then derive an approximate solution of (21) which yields [37]

$$k_B T_i(x) \simeq k_B T\sqrt{1+\frac{x}{x_s}} + \frac{N_b}{4\rho_o}\left(1 - e^{\frac{4k_B T}{N_b/\rho_o}\left[1-\sqrt{1+\frac{x}{x_s}}\right]}\right), \quad (22)$$

with $x_s = (\pi k_B T)^2\rho_o/(3\eta N_b)$. At short distances $x \ll x_s$, we have $T_i(x) \simeq T(1 + x/x_s)$, in which case the integral in (16) can be evaluated analytically, yielding

$$|\mathcal{F}_E(x)|^2 \simeq \exp\left[-\frac{2}{3}\frac{\eta k_B T}{(\hbar v_o)^2}\left(x^3 + \frac{x^4}{12 x_s}\right)\right], \quad \text{for } x \ll x_s. \quad (23)$$

Hence, the smaller the propagation velocity v_o, the stronger the dephasing, a trend which was recently observed by Gurman et al. [35]. At large distances $x \gg x_s$, the exponential term in Eq. (22) vanishes and $T_i(x) \simeq k_B T\sqrt{1 + x/x_s} + N_b/(4\rho_o)$.

From the data in [33], we can estimate that in the experiment, $N_b/\rho_o \approx 1.6\,\mu$eV [43]. The only remaining free parameter η can then be determined by fitting Eq. (19) to the measured visibility, using the experimentally determined values for the other parameters [33]: $k_B T \approx 31$ mK, $v_o \approx 5\cdot 10^4 \mathrm{ms}^{-1}$ and $r_1 = r_2 = t_1 = t_2 \approx 1/\sqrt{2}$, as well as $L_1 = L_2 = L \approx 7.2\,\mu$m. This yields [43] an energy drift velocity of $\eta \approx 2.8\,\mu\mathrm{eV}/\mu\mathrm{m}$. This value further justifies our perturbative analysis for weak momentum conservation breaking of the experiment [33], where a visibility independent of the injection energy is observed in the range $(E_0 - \mu_o) \in [30, 130]\,\mu\mathrm{eV} > \eta L \approx 28\,\mu eV$. The regime where $\eta L > E_0 - \mu_o$ is outside of the Fokker-Planck regime, since the distribution in the outer ES can no longer be separated into two non-overlapping contributions. Experimentally, dephasing in this regime is observed to depend on the injection energy [33]. Using the above estimates, we plot the visibility according to Eq. (19), with $\Delta L = 0$, as a function of the interferometer length in Fig. 2.

To further validate our analytic results, we compare them with the results from a Monte Carlo simulation of the Fokker-Planck dynamics of the kinetic equation, for different values of the injection energy. In this simulation, we discretize the stochastic energy exchange process for a given injection energy. At each step, we determine the scattering rate and the

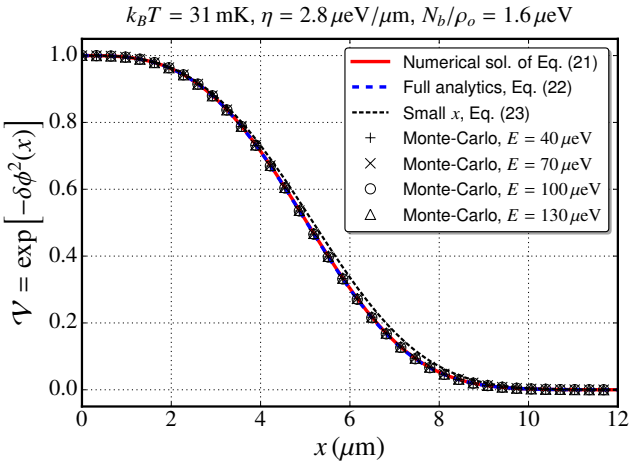
k_BT = 31 mK, η = 2.8 μeV/μm, N_b/ρ_o = 1.6 μeV
Numerical sol. of Eq. (21)
Full analytics, Eq. (22)
Small x, Eq. (23)
Monte-Carlo, E = 40 μeV
Monte-Carlo, E = 70 μeV
Monte-Carlo, E = 100 μeV
Monte-Carlo, E = 130 μeV
$\mathcal{V} = \exp\left[-\delta\phi^2(x)\right]$
x (μm)

FIG. 2. Visibility of the current interference fringes (19) as a function of the interferometer arm length for $\Delta L = 0$, $r_1 = r_2 = t_1 = t_2 = 1/\sqrt{2}$, and $v_o = 5{\cdot}10^4$ m/s. The solid (red) curve shows the result obtained by numerically integrating the differential equations (21). The dashed (blue) curve shows the analytic result obtained using Eq. (22). The thin dashed (black) curve shows Eq. (23), obtained from the short distance limit of (22), when $x \ll x_s \approx 5.2\,\mu$m. The symbols show results from Monte Carlo simulations of the kinetic equation for different injection energies $E \in \{40, 70, 100, 130\}\,\mu$eV [43].

distribution of scattering energies from Eq. (7). We then use these to update the energy and accumulated phase of an electron as it propagates along the edge. The phase suppression factor is estimated by averaging over many such "trajectories": $\mathcal{F}_E(x) = (1/M)\sum_{m=1}^{M} \exp(i\phi_{E,m}(x))$. Further details on our implementation are given in [43]. The results confirm our analytic predictions (see Fig. 2).

In conclusion, we have shown how the interplay of disorder and Coulomb interaction leads to the loss of phase coherence of the current through a MZI formed with two co-propagating ESs of the integer quantum Hall effect. Crucially we find that dephasing does not depend on the injection energy, in agreement with recent experiments [33]. Furthermore, our theory makes quantitative predictions for the length dependence of the dephasing (see Fig. 2 and Eqs. (16), (17) and (22)), which could easily be tested by adapting existing experimental systems.

Acknowledgments. We thank Karsten Flensberg for discussion. The Monte Carlo simulations were performed in a parallel computing environment at sciCORE (`http://scicore.unibas.ch/`) scientific computing core facility at University of Basel. SEN acknowledges financial support from the Swiss NSF and AML from the Carlsberg Foundation.

* Corresponding author: simon.nigg@unibas.ch

[1] D. C. Tsui, H. L. Stormer, and A. C. Gossard, Phys. Rev. Lett. **48**, 1559 (1982).
[2] X. G. Wen, Phys. Rev. B **41**, 12838 (1990).
[3] S. Das Sarma, M. Freedman, and C. Nayak, Phys. Rev. Lett. **94**, 166802 (2005).
[4] P.-A. Huynh, F. Portier, H. le Sueur, G. Faini, U. Gennser, D. Mailly, F. Pierre, W. Wegscheider, and P. Roche, Phys. Rev. Lett. **108**, 256802 (2012).
[5] E. Bocquillon, V. Freulon, F. D. Parmentier, J.-M. Berroir, B. Plaçais, C. Wahl, J. Rech, T. Jonckheere, T. Martin, C. Grenier, et al., Annalen der Physik **526**, 1 (2014).
[6] G. Haack, M. Albert, and C. Flindt, Phys. Rev. B **90**, 205429 (2014).
[7] P. P. Hofer and B. Sothmann, Phys. Rev. B **91**, 195406 (2015).
[8] R. Sánchez, B. Sothmann, and A. N. Jordan, Phys. Rev. Lett. **114**, 146801 (2015).
[9] B. I. Halperin, Phys. Rev. B **25**, 2185 (1982).
[10] M. Büttiker, Phys. Rev. B **38**, 9375 (1988).
[11] S. Komiyama, H. Hirai, S. Sasa, and S. Hiyamizu, Phys. Rev. B **40**, 12566 (1989).
[12] D. B. Chklovskii, B. I. Shklovskii, and L. I. Glazman, Phys. Rev. B **46**, 4026 (1992).
[13] R. J. F. van Haren, F. A. P. Blom, and J. H. Wolter, Phys. Rev. Lett. **74**, 1198 (1995).
[14] Y. Ji, Y. Chung, D. Sprinzak, M. Heiblum, D. Mahalu, and H. Shtrikman, Nature **422**, 415 (2003).
[15] F. Marquardt and C. Bruder, Phys. Rev. Lett. **92**, 056805 (2004).
[16] P. Roulleau, F. Portier, D. C. Glattli, P. Roche, A. Cavanna, G. Faini, U. Gennser, and D. Mailly, Phys. Rev. B **76**, 161309 (2007).
[17] L. V. Litvin, H.-P. Tranitz, W. Wegscheider, and C. Strunk, Phys. Rev. B **75**, 033315 (2007).
[18] P. Roulleau, F. Portier, P. Roche, A. Cavanna, G. Faini, U. Gennser, and D. Mailly, Phys. Rev. Lett. **101**, 186803 (2008).
[19] I. P. Levkivskyi and E. V. Sukhorukov, Phys. Rev. B **78**, 045322 (2008).
[20] H. le Sueur, C. Altimiras, U. Gennser, A. Cavanna, D. Mailly, and F. Pierre, Phys. Rev. Lett. **105**, 056803 (2010).
[21] C. Altimiras, H. le Sueur, U. Gennser, A. Cavanna, D. Mailly, and F. Pierre, Nature Physics **6**, 34 (2010).
[22] C. Altimiras, H. le Sueur, U. Gennser, A. Cavanna, D. Mailly, and F. Pierre, Phys. Rev. Lett. **105**, 226804 (2010).
[23] A. M. Lunde, S. E. Nigg, and M. Büttiker, Phys. Rev. B **81**, 041311 (2010).
[24] T. Otsuka, E. Abe, Y. Iye, and S. Katsumoto, Phys. Rev. B **81**, 245302 (2010).
[25] P. Degiovanni, C. Grenier, G. Fève, C. Altimiras, H. le Sueur, and F. Pierre, Phys. Rev. B **81**, 121302 (2010).
[26] D. L. Kovrizhin and J. T. Chalker, Phys. Rev. B **84**, 085105 (2011).
[27] I. P. Levkivskyi and E. V. Sukhorukov, Phys. Rev. B **85**, 075309 (2012).
[28] T. Karzig, A. Levchenko, L. I. Glazman, and F. von Oppen, New J. of Phys. **14**, 105009 (2012).
[29] L. Chirolli, F. Taddei, R. Fazio, and V. Giovannetti, Phys. Rev. Lett. **111**, 036801 (2013).
[30] T. Otsuka, Y. Sugihara, J. Yoneda, T. Nakajima, and S. Tarucha, J. of the Phys. Soc. of Japan **83**, 014710 (2014).
[31] H. Inoue, A. Grivnin, N. Ofek, I. Neder, M. Heiblum, V. Umansky, and D. Mahalu, Phys. Rev. Lett. **112**, 166801 (2014).
[32] A. Helzel, L. V. Litvin, I. P. Levkivskyi, E. V. Sukhorukov, W. Wegscheider, and C. Strunk, Phys. Rev. B **91**, 245419 (2015).
[33] S. Tewari, P. Roulleau, C. Grenier, F. Portier, A. Cavanna, U. Gennser, D. Mailly, and P. Roche, Phys. Rev. B **93**, 035420 (2016).

[34] A. O. Slobodeniuk, E. G. Idrisov, and E. V. Sukhorukov, Phys. Rev. B **93**, 035421 (2016).

[35] I. Gurman, R. Sabo, M. Heiblum, V. Umansky, and D. Mahalu, Phys. Rev. B **93**, 121412 (2016).

[36] N. Pascher, C. Rössler, T. Ihn, K. Ensslin, C. Reichl, and W. Wegscheider, Phys. Rev. X **4**, 011014 (2014).

[37] A. M. Lunde and S. E. Nigg, arxiv:1602.05039 (2016).

[38] M. Büttiker, Phys. Rev. Lett. **57**, 1761 (1986).

[39] Y. Blanter and M. Büttiker, Physics Reports **336**, 1 (2000).

[40] We neglect *intra*-ES interaction, because the direct and exchange terms within each spin polarized ES tend to cancel each other [23, 37, 43].

[41] Since the slope (normal derivative) of the confinement potential increases as one approaches the edge, one typically expects $v_o > v_i$.

[42] E. Bocquillon, V. Freulon, J.-. M. Berroir, P. Degiovanni, B. Plaçais, A. Cavanna, Y. Jin, and G. Fève, Nat Commun **4**, 1839 (2013).

[43] See supplemental material at [URL provided by publisher].

[44] C. W. Gardiner, *Handbook of stochastic methods for physics, chemistry, and the natural sciences* (Springer-Verlag, Berlin, 1983).

[45] When varying the path length difference instead of the flux, the given visibility is an approximation since the decay factor also depends on the path length difference. However, in the regime considered here, where $E_0 - \mu_o \gg \Gamma_0, \eta L_i$, the oscillation period is much shorter than the characteristic decay length and this approximation is justified.

[46] D. E. Knuth, *The Art of Computer Programming* (Addison-Wesley, 1998), 3rd ed.

[47] C. W. J. Beenakker, Phys. Rev. B **44**, 1646 (1991).

Supplementary Material for "Stochastic theory of interaction-induced decoherence of weakly disordered edge states"

Simon E. Nigg and Anders Mathias Lunde

This supplementary material contains further information to complement the main text. In particular, we provide: 1) An explicit model for the kinetic Boltzmann equation including momentum conservation breaking disorder. 2) A physically motivated Monte Carlo simulation of the energy exchange dynamics based on the kinetic Boltzmann equation. 3) A derivation of the identity (15) of the main text. 4) Details on the parameter estimation from the experimental data of Tewari et al. [33].

1. EFFECTIVE COULOMB INTERACTION KERNEL FOR DISORDERED EDGE STATES

While edge states of the integer quantum Hall effect are often described as translationally invariant one dimensional channels on length scales of hundreds of microns, recent scanning tunneling experiments in high mobility samples have detected edge roughness with a characteristic length scale of a few hundred nanometers [36].

Here we derive an effective Coulomb interaction kernel for inter-ES scattering, in the presence of translation invariance breaking disorder, which has the form used in the collision integral Eq. (7) of the main paper. This extends the earlier derivations given in [23 and 37].

Our starting point is the Boltzmann kinetic equation for the distribution functions of the inner and outer ESs in momentum space

$$v_\alpha \partial_x f_{\alpha,k}(x) = \sum_{k_2 k_{1'} k_{2'}} W_{12,1'2'} \Big\{ f_{1'}(x)[1-f_1(x)] f_{2'}(x)[1-f_2(x)] - f_1(x)[1-f_{1'}(x)] f_2(x)[1-f_{2'}(x)] \Big\}, \tag{24}$$

where we use the shorthand notation $1 = \alpha, k_1$ and $2 = \bar{\alpha}, k_2$ and $\alpha \in \{i, o\}$ and $\bar{\alpha} = o\delta_{\alpha i} + i\delta_{\alpha o}$. The interaction kernel is obtained via Fermi's golden rule and reads

$$W_{12,1'2'} = \frac{2\pi}{\hbar} |\langle k_{1'}\alpha, k_{2'}\bar{\alpha}|V|k_1\alpha, k_2\bar{\alpha}\rangle|^2 \delta(E_{k_1\alpha} + E_{k_2\bar{\alpha}} - E_{k_{1'}\alpha} - E_{k_{2'}\bar{\alpha}}), \tag{25}$$

The delta function in energy enforces energy conservation during the collision. Here V is the Coulomb interaction operator, the relevant matrix elements for inter-ES scattering of which are given by

$$\begin{aligned} V_{12,1'2'} &\equiv \langle k_{1'}\alpha, k_{2'}\bar{\alpha}|V|k_1\alpha, k_2\bar{\alpha}\rangle \\ &= \int dx_1 dx_2 \int dy_1 dy_2 \psi^*_{1'}(x_1, y_1)\psi^*_{2'}(x_2, y_2) V_C(x_1 - x_2, y_1 - y_2)\psi_1(x_1, y_1)\psi_2(x_2, y_2). \end{aligned} \tag{26}$$

Here

$$\psi_{k,\alpha}(x, y) = \frac{1}{\sqrt{L}} e^{ik_\alpha x} \frac{1}{\pi^{1/4}\sqrt{\ell_B}} \exp\left[-\frac{(y - y_\alpha(x))^2}{2\ell_B^2} \right], \tag{27}$$

is the wavefunction of an electron in ES α, which is localized in the transverse direction to within the magnetic length $\ell_B = \sqrt{\hbar/(|e|B)}$, on the guiding center coordinate $y_\alpha(x)$. Disorder will be included in the dependence of the guiding center coordinate on the longitudinal coordinate x, as explained further below. Note that we suppress the spin index, keeping in mind that the two edge states have opposite spins. Because of this, the exchange term is absent for inter-ES interaction. For *intra*-ES interaction, both direct and exchange terms are present (since the ESs are spin polarized), and typically compensate each other. In a model with contact interaction, such as used below, this cancellation is complete, resulting in a vanishing matrix element. In general, the cancellation is not exact, but for sufficiently short range interaction, the inter-ES interaction dominates over the intra-ES interaction, justifying neglecting the latter [23, 37]. L denotes the length of the system in the propagation direction. The Coulomb potential energy in the plane of the 2DEG at $z = 0$ is

$$V_C(x_1 - x_2, y_1 - y_2) = \frac{e^2}{4\pi\epsilon_0} \frac{e^{-\sqrt{(x_1-x_2)^2 + (y_1-y_2)^2}/\ell_s}}{\sqrt{(x_1 - x_2)^2 + (y_1 - y_2)^2}}. \tag{28}$$

Here we include screening by the metallic gates with characteristic screening length ℓ_s. Substituting into Eq. (26) yields

$$V_{121'2'} = \frac{1}{L^2}\frac{e^2}{4\pi\epsilon_0}\int dx_1 dx_2 e^{i(k_1-k_{1'})x_1+i(k_2-k_{2'})x_2} \times \frac{1}{\pi\ell_B^2}\int dy_1 dy_2 \frac{e^{-\sqrt{(x_1-x_2)^2+(y_1-y_2)^2}/\ell_s}}{\sqrt{(x_1-x_2)^2+(y_1-y_2)^2}} \exp\left[-\frac{[y_1-y_\alpha(x_1)]^2}{\ell_B^2}\right]\exp\left[-\frac{[y_2-y_{\bar\alpha}(x_2)]^2}{\ell_B^2}\right]. \tag{29}$$

To make further progress we now assume that $\ell_B \ll \ell_s$, in which case we can approximate the Gaussians by delta functions and perform the integrals over y_1 and y_2 to obtain

$$V_{121'2'} \simeq \frac{1}{L^2}\frac{e^2}{4\pi\epsilon_0}\int dx_1 dx_2 e^{i(k_1-k_{1'})x_1+i(k_2-k_{2'})x_2}\frac{e^{-\sqrt{(x_1-x_2)^2+[y_\alpha(x_1)-y_{\bar\alpha}(x_2)]^2}/\ell_s}}{\sqrt{(x_1-x_2)^2+[y_\alpha(x_1)-y_{\bar\alpha}(x_2)]^2}}. \tag{30}$$

Next, we introduce the relative and center of mass coordinates $r = (x_1 - x_2)/2$ and $R = (x_1 + x_2)/2$, and write $y_\alpha(x_1) - y_{\bar\alpha}(x_2) = \Delta y_0 + \delta y(r, R)$, where the disorder induced deviation is small in the sense that $|\delta y(r, R)| \ll \Delta y_0$. Then

$$V_{121'2'} = \frac{1}{L^2}\frac{e^2}{4\pi\epsilon_0}\int dr dR e^{i\Delta q r + i\Delta k R}\frac{e^{-\sqrt{(2r)^2+[\Delta y_0+\delta y(r,R)]^2}/\ell_s}}{\sqrt{(2r)^2+[\Delta y_0+\delta y(r,R)]^2}}, \tag{31}$$

with $\Delta q = k_1 - k_2 - k_{1'} + k_{2'}$ and $\Delta k = k_1 + k_2 - k_{1'} - k_{2'}$. If we assume that the momentum exchanges are small, in the sense that $\Delta q \ell_s \ll 1$, then we can approximate the integral over r by ℓ_s times the integrand at $r = 0$, which yields

$$\begin{aligned} V_{121'2'} &\simeq \frac{\ell_s}{L^2}\frac{e^2}{4\pi\epsilon_0}\int dR e^{i\Delta k R}\frac{e^{-[\Delta y_0+\delta y(R)]/\ell_s}}{\Delta y_0+\delta y(R)} \\ &\simeq \frac{1}{L^2}\frac{e^2}{4\pi\epsilon_0}\frac{\ell_s e^{-\Delta y_0/\ell_s}}{\Delta y_0}\int dR e^{i\Delta k R}(1-\delta y(R)/\ell_s), \end{aligned} \tag{32}$$

where $\delta y(R) = \delta y(0, R)$ and, in the last step, we have assumed that $|\delta y(R)| \ll \ell_s$. Thus the matrix elements splits into the sum of two contributions. The first one, which is proportional to $\frac{1}{L}\int dR e^{i\Delta k R} = \delta_{0\Delta k}$, represents the momentum conserving part of the scattering. Because, for linear dispersion with different ES velocities, inelastic collisions conserving both momentum and energy are forbidden, this term does not contribute to the kernel. The second contribution to the matrix element is proportional to $\int dR e^{i\Delta k R}\delta y(R)$ and its contribution to the kernel will in general not vanish in the presence of disorder (i.e. for $\delta y(R) \neq$ const). The function $\delta y(R)$ depends on the particular realization of disorder. Since we are not interested in a specific disorder realization, we model its effect by assuming Gaussian correlated fluctuations, i.e.

$$\langle \delta y(R)\rangle_{\text{disorder}} = 0, \quad \langle \delta y(R)\delta y(R')\rangle_{\text{disorder}} = \frac{A}{\sqrt{2\pi}\ell_p}\exp\left[-\frac{(R-R')^2}{2\ell_p^2}\right]. \tag{33}$$

Here $\sqrt{A/\ell_p}$ determines the maximum magnitude of the transverse fluctuations while the momentum conservation breaking correlation length ℓ_p, characterizes the edge roughness in the propagation direction ($\ell_p \to \infty$ for a translation invariant system). With this model of disorder, we can now compute the relevant disorder averaged squared matrix element for non-momentum conserving scattering

$$\langle |V^{(\Delta k\neq 0)}_{121'2'}|^2\rangle_{\text{disorder}} = \left(\frac{1}{L^2}\frac{e^2}{4\pi\epsilon_0}\frac{e^{-\Delta y_0/\ell_s}}{\Delta y_0}\right)^2\frac{A}{\sqrt{2\pi}\ell_p}\int dR dR' e^{i\Delta k(R-R')}\exp\left[-\frac{(R-R')^2}{2\ell_p^2}\right] \simeq \frac{A}{L^3}\left(\frac{e^2}{4\pi\epsilon_0}\frac{e^{-\Delta y_0/\ell_s}}{\Delta y_0}\right)^2 e^{-(\Delta k\ell_p)^2/2}. \tag{34}$$

Using the dispersion relation $k_\alpha = \frac{E_\alpha}{\hbar v_\alpha}$ and energy conservation $E_1 + E_2 - E_{1'} - E_{2'} = 0$, we can write $\Delta k\ell_p/\sqrt{2} = \omega/\Delta E$, with

$$\omega = E_1 - E_{1'} = E_{2'} - E_2, \tag{35}$$

$$\Delta E = \frac{\sqrt{2}}{\ell_p}\frac{\hbar v_i v_o}{|v_i - v_o|}. \tag{36}$$

Substituting into Eq. (24) and changing from discrete momentum summation to continuum integration over energy ($\sum_{k_\alpha} \to \frac{L}{\hbar v_\alpha}\int dE$), we finally obtain after some algebra

$$\partial_x f_\alpha(x) = \gamma\int_{-\infty}^{\infty} d\omega e^{-(\omega/\Delta E)^2}\Big\{f_\alpha(E+\omega,x)[1-f_\alpha(E,x)]D_{\bar\alpha}(\omega,x) - f_\alpha(E,x)[1-f_\alpha(E+\omega,x)]D_{\bar\alpha}(-\omega,x)\Big\}, \tag{37}$$

with

$$\gamma = \frac{2\pi A}{(\hbar v_i \hbar v_o)^2} V_0^2, \quad V_0 = \frac{e^2}{4\pi\epsilon_0} \frac{e^{-\Delta y_0/\ell_s}}{\Delta y_0}, \tag{38}$$

and $D_\alpha(\omega, x) = \int_{-\infty}^{\infty} dE' f_\alpha(E' - \omega, x)[1 - f_\alpha(E', x)]$. In conclusion, we have derived an effective model for Coulomb interaction between two weakly disordered ESs. A few comments to conclude: Firstly, the divergence of ΔE for $v_i = v_o$ is an artifact of using a linear dispersion relation. A linear dispersion relation is not essential for the momentum conservation breaking physics but is convenient for computations. Furthermore, in general one can expect that $v_o > v_i$, since the outer ES is closer to the edge of the sample. Secondly, we note that $V_0 \to 0$ for $\ell_s \ll \Delta y_0$. This is intuitively reasonable, since the edge states are separated by a finite distance $\sim \Delta y_0$ and if the screening is too strong, electrons on the inner and outer ESs do not interact. Finally, we note that Eq. (37) can be obtained directly [23, 37], by starting with an effective one-dimensional local inter-ES interaction potential of the form $V_{\text{eff}}(x, x') = V_0 g(x)\delta(x - x')$, with $\langle (g(x) - g_0)(g(x') - g_0)\rangle = A/(\sqrt{2\pi}\ell_p) \exp[-(x - x')^2/(2\ell_p^2)]$ and $g_0 = \langle g(x)\rangle$.

2. MONTE CARLO SIMULATION

In this section we describe a Monte Carlo simulation of the Fokker-Planck dynamics described by the kinetic Eq. (6) and (7) of the main text. This simulation is based on discretizing the stochastic energy exchange process in space. To form a qualitative picture, imagine following an injected electron as it propagates along the outer ES. At random times $t_i = v_o x_i$, it will scatter off an electron in the inner ES, changing its energy and thereby the phase accumulation rate. The phase at a given distance is then a random number given by the sum of the phases accumulated in every interval up to that distance. Importantly, both the scattering rate and the scattering energy probability distribution depend on position and need to be updated in each interval. Next we describe in detail how this is achieved.

We want to compute numerically the expectation value of a function $\xi(\phi_E)$ of the phase ϕ_E accumulated by an electron, with initial energy E, propagating in the outer ES along one arm of the MZI. Let L denote the total arm length. From the kinetic Eq. (6) and (7) of the main text, the number of scattering events per length for an electron at position x is

$$S(x) = \gamma \int_{-\infty}^{\infty} d\omega e^{-\left(\frac{\omega}{\Delta E}\right)^2} [1 - b(E, x)]\, D_i(\omega, x) \simeq \gamma \int_{-\infty}^{\infty} d\omega e^{-\left(\frac{\omega}{\Delta E}\right)^2} D_i(\omega, x) \simeq \gamma \sqrt{\pi} \Delta E D_i(0, x), \tag{39}$$

where the middle expression holds in the Fokker-Planck limit where $b(E, x) \ll 1$ and the last expression holds for weak momentum conservation breaking, where ΔE is the smallest energy scale.

It can further be easily shown that the scattering probability density from energy E to E' at position x is

$$P_{E\to E'} = \frac{e^{-\left(\frac{E-E'}{\Delta E}\right)^2} D_i(E - E', x)}{\int_{-\infty}^{\infty} dE' e^{-\left(\frac{E-E'}{\Delta E}\right)^2} D_i(E - E', x)}. \tag{40}$$

Finally, within the effective temperature approximation (see Eq. (20) of the main text)

$$D_i(E - E', x) \simeq \frac{E - E'}{1 - \exp\left[-\frac{E-E'}{k_B T_i(x)}\right]}. \tag{41}$$

The Monte-Carlo algorithm we implement is now as follows: We discretize the length of the interferometer arm into segments of size $\Delta x = L/N$ with some suitably large integer N such that $\Delta x S(x) < 1$. Then, $\Delta x S(x)$ gives the scattering probability in the interval $[x, x + \Delta x]$. Using the Metropolis-Hastings algorithm, in every interval $n = 0 \ldots N - 1$, we draw a uniformly distributed random number $r_n \in [0, 1)$ and if $\Delta x S(n\Delta x) > r_n$, we scatter the electron's energy by drawing a random number E' from the distribution $P_{E_n \to E'}$, i.e. $E((n + 1)\Delta x) = E'$, otherwise we leave the energy unchanged, i.e. $E((n + 1)\Delta x) = E(n\Delta x) \equiv E_n$. The accumulated phase for one such "trajectory" from $x = 0$ to $x = N\Delta x = L$ is then approximated by

$$\phi_E = \frac{\Delta x}{\hbar v_o} \sum_{n=0}^{N-1} E(n\Delta x). \tag{42}$$

The injection energy is given by the initial condition $E(0) = E$. We repeat this loop M times and estimate the sample average and variance of $\xi(\phi)$ according to Knuth's online algorithm (See. e.g. [46]). In Fig. (2) of the main text, we show the resulting visibility for an interferometer with equal arm lengths x, $\mathcal{V}(x) = |\mathcal{F}_E(x)|^2 = |\frac{1}{M} \sum_m \exp(i\phi_{E,m}(x))|^2$, for different values of the injection energy and $M = 40000$ trajectories per energy. The Monte Carlo simulation results perfectly confirm our analytic predictions to within the statistical uncertainty $\sim 1/\sqrt{M} = 0.5\%$.

The code of our implementation is written in python 3 using the numerical libraries numpy and scipy and is made available for inspection upon request. Please send inquiries to simon.nigg@unibas.ch.

3. DOUBLE INTEGRAL WITH STOCHASTIC TERM

Here we prove Eq. (15) of the main text. Consider the stochastic integral

$$K_y = \int_0^y g(z)\mathrm{d}W_z. \tag{43}$$

Using Itô's calculus we have

$$d(K_y y) = \mathrm{d}K_y y + K_y dy + \mathrm{d}K_y dy. \tag{44}$$

Because $\mathrm{d}K_y = g(y)\mathrm{d}W_y$ and since $\mathrm{d}W_y dy = 0$, we simply have, as in normal calculus

$$\int_0^x \int_0^y g(z)\mathrm{d}W_z dy = \int_0^x K_y dy = \int_0^x \left[d(K_y y) - \mathrm{d}K_y y\right] = K_x x - \int_0^x y g(y)\mathrm{d}W_y = \int_0^x (x-y)g(y)\mathrm{d}W_y. \tag{45}$$

4. ESTIMATION OF PARAMETERS FROM EXPERIMENTAL DATA

Here we explain in more details how we estimated the parameters η and N_b/ρ_o from the experimental data presented in [33]. The transmission probability of the injection QD is given in Fig. 2(b) of [33] and fits with that of a thermally broadened QD level given by [47]

$$P_{\text{transmission}} = H \cosh^{-2}\left(\frac{E_0 - \mu_o}{2k_{\text{B}}T}\right), \tag{46}$$

with electronic temperature $T \approx 31$ mK. $E_0 - \mu_o$ is the energy difference between the QD energy level (average injection energy) and the Fermi energy of the outer ES. The maximal measured transmission probability is $H \approx 0.15$. The parameter N_b/ρ_o is then simply given by the integral of the transmission curve, that is

$$\frac{N_b}{\rho_o} = \int dE_0 P_{\text{transmission}} = 4Hk_{\text{B}}T \approx 1.6\,\mu\text{eV}. \tag{47}$$

Having determined N_b/ρ_o, the only remaining free parameter is η. An estimate for the latter is obtained by fitting the visibility as follows. Since the interferometer used in [33] is approximately symmetric, we assume equal arm lengths $\Delta L = 0$. Furthermore, in the experiment the QPCs are tuned to be semi-transparent, i.e. $r_1 = r_2 = t_1 = t_2 = 1/\sqrt{2}$. According to Eq.(19) of the main text, the visibility is then simply given by the absolute value squared of the coherence suppression factor i.e.

$$\mathcal{V}(x) = |\mathcal{F}_E(\phi)|^2 = e^{-\delta\phi^2(x)}. \tag{48}$$

The variance of the phase is given by Eq. (16) of the main text and in the effective temperature approximation is

$$\delta\phi^2(x) = \frac{2\eta k_{\text{B}}}{(\hbar v_o)^2}\int_0^x (x-y)^2 T_i(y)dy. \tag{49}$$

Here, the effective temperature $T_i(x)$ is determined by the system of differential equations (22) of the main text and thereby depends on η and N_b/ρ_o.

In the energy range $30\,\mu\text{eV} < E_0 - \mu_o < 120\,\mu\text{eV}$ the measured visibility is independent of the injection energy and its mean value is approximately [33]

$$\mathcal{V}(L) \approx 0.125, \tag{50}$$

where $L \approx 7.2\,\mu$m, is the arm length of the interferometer (See caption of Fig. 1 in [33]). We compute numerically $\mathcal{V}(L)$ according to Eqs. (48) and (49) and plot the solution as a function of η in Fig. 3. Comparing with Eq. (50) we find that the value of the energy drift velocity consistent with the experiment is

$$\eta \approx 2.8\,\frac{\mu\text{eV}}{\mu\text{m}}. \tag{51}$$

With these parameters thus determined, we find for the crossover distance defined in the main text $x_s = (\pi k_{\text{B}}T)^2\rho_o/(3\eta N_b) \approx 5.2\,\mu$m.

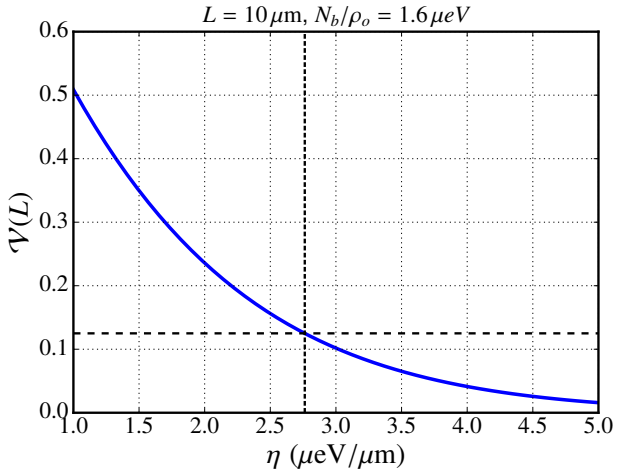

FIG. 3. Graphical determination of the energy drift velocity. The (blue) solid curve is computed by solving numerically the differential equations (21) of the main text for the effective temperature $T_i(x)$. The horizontal (black) dashed line gives the value of the visibility measured in [33] and the vertical (black) dashed line indicates the fitting value of η.